International Journal of Multimedia and Ubiquitous Engineering
Vol.11, No.5 (2016), pp.21-30
http://dx.doi.org/10.14257/ijmue.2016.11.5.03

3D Unsteady Simulation of the Transport Characteristics in the LEC Melt of In-Doped GaAs

Shuxian Chen[1, 2, a,]*, Shilin Li [1, b] and Xiaoming Tan [2, c]

[1]*Aviation Engineering Institute, Civil Aviation Flight University of China, Guanghan, 618307, China*
[2]*Jiangsu Province Key Laboratory of Aerospace Power Systems, Nanjing University of Aeronautics and Astronautics, Nanjing, 210016, China*
[a]*Bellesavana@163.com,* [b]*5423481@qq.com,* [c]*txmyy@nuaa.edu.cn*
** Corresponding Author: Shuxian Chen*

Abstract

A three-dimensional and time-dependent turbulent mathematical model is established for the mass, heat, momentum and dopant transport in the LEC melt of In-doped GaAs. The Solution scheme for the dopant segregation effect at the melt/crystal interface is put forward. Grid testing calculations have been performed for the choice of the grid. The turbulent mathematical model and numerical methodology are used to simulate the melt convections and dopant transports in the previously published experiments, and the numerical accuracy is validated by comparing the results with the experimental data in different model setups. Some transport characteristics in the LEC melt of In-doped GaAs have been concluded. Owing to the interacting forces associated with different length scales in the LEC melt, the fluid flow is non-axisymmetric. Because of the competition between buoyancy, Marangoni force, centrifugal force and the Coriolis force, the temperature fluctuates in the melt. Due to the segregation, the InAs concentration increase in the axial direction.

Keywords*: Computer simulation, transport characteristics, LEC melt, In-doped GaAs*

1. Introduction

GaAs single crystal is the most important semiconducting material for the production of optoelectronic devices and high-speed electronic circuits and usually grown by the LEC (liquid-encapsulated Czochralski) method. The LEC growth technique is in fact a modified Czochralski (Cz) process in which the melt is covered by a highly viscous encapsulate, generally B_2O_3, to prevent the separation of the volatile component at the melt surface. In a typical LEC growth furnace, the heat and mass transport and the fluid dynamics in the melt are quite complex because of their highly nonlinear and strongly coupled interactions, and also are extremely important in the vicinity of the crystallization front and therefore influences the quality of the crystal [8]. High dislocation density and strong dopant inhomogeneities that deteriorate the device performance have been found in LEC grown GaAs crystals. The origin and underlying mechanisms of these defects are attributed to the complex nature of transport phenomena in the LEC melt of GaAs [1].

So, understanding the heat, mass and momentum transport characteristics in the LEC melt of GaAs is of great importance. Due to the complex interactions of buoyancy, centrifugal and Coriolis force, the main features of the flow in the LEC melt of GaAs are still not well understood. Numerical simulation has become a useful tool for understanding and optimization of physical mechanisms during

ISSN: 1975-0080 IJMUE

crystal growth in general and during the LEC growth in particular because an experimental approach is often hardly applicable and sufficiently expensive due to high temperatures and complexity of growth apparatuses [10]. Improvement of numerical tools also allows to examine extensive parameter sets in a shorter time, which facilitates a considerable reduction of development costs.

For the GaAs LEC crystal growth, there are a number of papers simulating melt convection in 2D [1] and 3D [15] approximations. A difficulty in simulating the melt flow is the fact that the flow usually has turbulent structure, which necessitates an application of a special turbulence model in the range of the Reynolds averaged Navier–Stokes equations (RANS) [11]. Vizman *et al*. has used a standard k-ε model with wall functions at solid boundaries to simulate the turbulent heat transfer and flow in the GaAs melt [15]. Yakovlev *et al*. [16] have chosen the low-Reynolds number k-ε turbulence model proposed by Jones and Launder [4] to describe turbulent mixing in the GaAs melt. Smirnova *et al*. [12] have applied the turbulence model of Spalart and Allmaras [13] for the calculation of the turbulent effective viscosity v_t in the GaAs melt. But the accuracy of either turbulence model for quantitative prediction of turbulent convection and heat transfer in the LEC GaAs melt has not been validated, and it remains unclear today what mathematical model is required to predict the transport properties in the LEC melt of GaAs.

In Addition, GaAs crystal has low resolved shear stress and is easy to generate and multiply dislocations due to thermal stress during the LEC growth, so that it is an important technical problem to reduce the dislocations as low as possible. One of the methods to grow low-dislocation density crystals is to increase the crystal resistance to thermal stress by doping impurity atoms [7]. GaAs single crystals have been doped with in to reduce dislocations by dramatically increasing the critically resolved shear stress, and they are called In-doped GaAs. The wide gap between the liquidus and solidus lines of the phase diagram causes severe macrosegregation to occur [3]. The effective segregation coefficient, k, for In in In-doped GaAs is much less than one (about 0.1-0.13) [2], and hence the solute is rejected into the melt during the solidification process. This increases the solute concentration in the melt near the melt/crystal interface. To address this issue, an approximate scheme should be employed.

In this study, 3D unsteady calculation model and numerical methodology for the simulation of the turbulent flow, heat and dopant transport, and segregation effect in the LEC GaAs melt is presented, and the accuracy of the simulation is validated by quantitative comparison with the available experimental results.

2. Physical and Mathematical Model

2.1 Physical Model

The schematic diagram adopted in the present simulation is shown in Figure 1. The crucible contains GaAs melt with height H and radius R_c. The crystal, represented by a copper disc, has a constant radius R_s. The crystal rotates at an angular velocity Ω_s in the counter-clockwise direction and the crucible rotates at an angular velocity Ω_c in the clockwise direction from a top view. The melt/crystal interface is assumed flat with the melting temperature T_m. The bottom wall of the crucible is adiabatic and the inside wall of the crucible is at a fixed temperature of T_c. The melt/encapsulant interface is assumed to be plane and has a radiate heat exchange with the ambient environment with a temperature of T_g. The Marangoni force at the melt/encapsulant interface is taken into account. No-slip boundary conditions are applied on all the rigid boundaries. As the initial conditions for the melt, zero velocity components and a homogeneous temperature distribution with

$T_{init}=0.5(T_m+T_c)$ are assigned. The thermo-physical properties of GaAs melt and the processing parameters used here are referred to ref. [6].

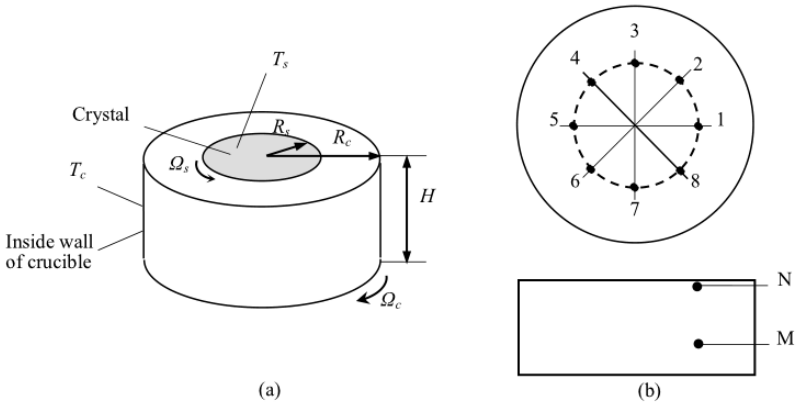

Figure 1. Schematic Illustration of the Calculating Model for the Melt in the LEC GaAs Crystal Growth Configuration (A) and the Arrangement of Monitor Points (B)

To describe the melt convection characteristics, at two vertical positions z=0.018 m and z= 0.0595 m indicated by indices of M and N, eight monitor points are located at the same radial position r=0.038 m, separated azimuthally by □=□/4 in the counter-clockwise direction as shown in Figure 1(b). The melt flow in the convection cell is characterized by the Grashof number $Gr=g\square H^3\square T/v^2$, crystal rotational Reynolds number $Re_s=\Omega_s(R_c-R_s)H/v$, crucible rotational Reynolds number $Re_c=\Omega_c R_c H/v$, and Marangoni number $Ma=\square_T\square T\ (R_c\square R_s)\ /\square v^2$, where g is the gravitational acceleration, □ the volumetric thermal expansion coefficient of GaAs melt, □T the temperature difference between the crystal and the side-wall of the crucible, v the kinematic viscosity, $\square_T$ the surface tension temperature coefficient, and □ the density of GaAs melt. The calculation is carried out in the following parameter ranges: Gr=1.665×10^7~6.66×10^7, Ma=3.306×10^5~ 1.322×10^6, Re_s=0~6.086×10^4, Re_c= 0~ 1.5457 ×10^4.

2.2 Governing Equations and Turbulence Models

Because the Grashof number Gr is of the order of 10^7, the flow in the melt is turbulent [9]. The flow and heat transfer in the melt are governed by the three-dimensional Reynolds-averaged equations for an incompressible melt expressing the conservation of mass, momentum and energy. The Boussinesq approximation is applied. The Reynolds stress tensor in the Reynolds-average equations of motion is described using the k-ε model formulation. The low-Reynolds number k-ε model proposed by Jones and Launder is used here. In a cylindrical coordinate system centered at the bottom of the crucible, the governing equations and the constitutive relationship can be written as follows:

$$\nabla\cdot V = S_1 \tag{1}$$

$$\frac{\partial(\rho u)}{\partial t}+\nabla\cdot(\rho V u)=\nabla\cdot(\mu_{eff}\nabla u)-\frac{\partial p}{\partial r}+\frac{\partial}{\partial z}(\mu_{eff}\frac{\partial v}{\partial r})+\frac{1}{r}\frac{\partial}{\partial r}(r\mu_{eff}\frac{\partial u}{\partial r}) \tag{2}$$
$$+\frac{1}{r}\frac{\partial}{\partial\theta}[\mu_{eff}\frac{r\partial(w/r)}{\partial r}]-\frac{2\mu_{eff}}{r}(\frac{1}{r}\frac{\partial w}{\partial\theta}+\frac{u}{r})+\frac{\rho w^2}{r}$$

$$\frac{\partial(\rho v)}{\partial t}+\nabla\cdot(\rho V v)=\nabla\cdot(\mu_{eff}\nabla v)-\frac{\partial p}{\partial z}+\frac{\partial}{\partial z}(\mu_{eff}\frac{\partial v}{\partial z})+\frac{1}{r}\frac{\partial}{\partial r}(r\mu_{eff}\frac{\partial u}{\partial z}) \tag{3}$$
$$+\frac{1}{r}\frac{\partial}{\partial\theta}(\mu_{eff}\frac{\partial w}{\partial z})-\rho g\beta(T-T_{ref})$$

$$\frac{\partial(\rho w)}{\partial t}+\nabla\cdot(\rho V w)=\nabla\cdot(\mu_{eff}\nabla w)-\frac{1}{\mathrm{r}}\frac{\partial p}{\partial\theta}+\frac{\partial}{\partial z}(\mu_{eff}\frac{\partial v}{r\partial\theta})+\frac{1}{r}\frac{\partial}{\partial r}[r\mu_{eff}(\frac{1}{r}\frac{\partial u}{\partial\theta}-\frac{w}{r})] \tag{4}$$
$$+\frac{1}{r}\frac{\partial}{\partial\theta}[\mu_{eff}(\frac{1}{r}\frac{\partial w}{\partial\theta}+\frac{2u}{r})]+\frac{\mu_{eff}}{r}[r\frac{\partial(w/r)}{\partial r}+\frac{1}{r}\frac{\partial v}{\partial\theta}]-\frac{\rho uv}{r}$$

$$\frac{\partial(\rho c_P T)}{\partial t}+\nabla\cdot(\rho V c_P T)=\nabla\cdot(k_{eff}\nabla T) \tag{5}$$

$$\frac{\partial(\rho C_m)}{\partial t}+\nabla\cdot(\rho V C_m)=\nabla\cdot(D_{eff}\nabla C_m)+S_2 \tag{6}$$

$$\frac{\partial(\rho k)}{\partial t}+\nabla\cdot(\rho V k)=\nabla\cdot[(\mu+\frac{\mu_t}{\sigma_k})\nabla k]+G_k+G_b-\rho\varepsilon-2\mu[(\frac{\partial k^{1/2}}{\partial r})^2+(\frac{\partial k^{1/2}}{\partial z})^2+(\frac{\partial k^{1/2}}{r\partial\theta})^2] \tag{7}$$

$$\frac{\partial(\rho\varepsilon)}{\partial t}+\nabla\cdot(\rho V\varepsilon)=\nabla\cdot[(\mu+\frac{\mu_t}{\sigma_\varepsilon})\nabla\varepsilon)]+\frac{\varepsilon}{k}[c_{1\varepsilon}f_1G_k-c_{1\varepsilon}G_b-c_{2\varepsilon}|f_2|\rho\varepsilon] \tag{8}$$

$$\mu_t=c_\mu f_\mu\rho k^2/\varepsilon \tag{9}$$

Where V represent velocity vector $(V_r,V_z,V_\theta)=(u,v,w)$; u,v and w denote velocity component in r,z and θ directions, respectively; p the static pressure; T the temperature of the melt; T_{ref} the reference temperature for the Boussinesq approximation; C_m the In dopant concentration in the GaAs melt; k the turbulent kinetic energy; ε the dissipation rate of turbulent energy; μ_{eff} the effective turbulent viscosity calculated as $\mu_{eff}=\mu+\mu_t$, μ the dynamic molecular viscosity, μ_t the turbulent viscosity; k_{eff} the effective heat conductivity calculated by $k_{eff}=\mu c_p/Pr+\mu_t c_p/\sigma_t$, c_p the specific heat, Pr the Prandtl number, σ_t the turbulent Prandtl number; and D_{eff} the effective diffusivity coefficient calculated by $D_{eff}=\mu/Sc+\mu_t/Sc_t$, Sc the Schmidt number, Sc_t the turbulent Schmidt number. The terms G_k representing the generation of turbulence kinetic energy due to the mean velocity gradients, G_b representing the generation of turbulence kinetic energy due to buoyancy, and the damping functions f_1, f_2 and f_μ used in the Jones-Launder form of the low-Reynolds model are referred to Ref. [14]. S_1 and S_2 are the source terms of mass transport equation and dopant composition transport equation, respectively.

All the constants $c_{1\varepsilon}$, $c_{2\varepsilon}$, c_μ, σ_k, σ_ε and σ_t in governing equations have the generally agreed values [14]:

$$c_{1\varepsilon}=1.44,\ c_{2\varepsilon}=1.92,\ c_\mu=0.09,\ \sigma_k=1.0,\ \sigma_\varepsilon=1.3,\ \sigma_t=0.9. \tag{10}$$

2.3 Solution Scheme for Segregation at the Melt/Crystal Interface

Following the method adopted by Zou *et al.* [10], the Dopant segregation at the melt/crystal interface is considered as the internal source terms of mass and species transport equations in the first control volume next to the crystal. In Zou *et al.*'s study [18], the segregation phenomenon was regarded as solute rejection to the melt from crystal at a rate $(1-k_{eff})V_{\mathrm{pull}}C_{\mathrm{m}}$ causing the increase of solute, and a positive internal source term,

$$S_d=(1-k_{eff})C_m\rho_s V_{pull}A/vol, \tag{11}$$

Was introduced to the species transport equation, where $k_{eff}=C_s/C_m$ is the effective segregation coefficient for In in In-doped GaAs, C_s the In dopant concentration in the GaAs crystal, ρ_s the density of the GaAs crystal, V_{pull} the crystal pulling speed, $\boldsymbol{A}$ the normal area and vol the control volume next to the melt/crystal interface.

However, both the melt and the dopant are decreased during crystal puling process. So the segregation phenomenon could rather be regard as a sink in the first control volume in the melt near the melt/crystal interface, and the dopant concentration involved in crystal because of solidification is less than that in the

melt, which causing the increase of dopant concentration in the melt. As a result, two negative source terms S_1 and S_2 are introduced to the mass and species transport equations respectively in the present study:

$$S_1 = -\rho_s V_{pull} \pi R_s^2 / vol\,, \tag{12}$$

$$S_2 = -k_{eff} C_m \rho_s V_{pull} \pi R_s^2 / vol \tag{13}$$

2.4 Boundary Conditions

At the melt/crystal interface:

$$u = 0,\ v = 0,\ w = \Omega_s r,\ T = T_m,\ -D\rho_m \nabla C_m \cdot n = C_m \rho_s (1 - k_{eff}) V_{pull} \cdot n,\ k = \varepsilon = 0 \tag{14a-f}$$

At the inside wall of the crucible:

$$u = 0,\ v = 0,\ w = \Omega_c R_c,\ T = T_c,\ \nabla C_m \cdot n = 0,\ k = \varepsilon = 0 \tag{15 a-f}$$

At the bottom of the crucible:

$$u = 0,\ v = 0,\ w = \Omega_c r,\ \frac{\partial T}{\partial z} = 0,\ \nabla C_m \cdot n = 0,\ k = \varepsilon = 0 \tag{16a-f}$$

At the melt/encapsulant interface:

$$\mu \frac{\partial u}{\partial z} = -\gamma_T \frac{\partial T}{\partial r},\ v = 0,\ \mu \frac{\partial w}{\partial z} = -\gamma_T \frac{\partial T}{r \partial \theta}, \tag{17 a-c}$$

$$-\lambda \frac{\partial T}{\partial z} = \varepsilon_T \sigma (T^4 - T_g^4),\ \nabla C_m \cdot n = 0,\ \frac{\partial k}{\partial z} = \frac{\partial \varepsilon}{\partial z} = 0 \tag{18 d-f}$$

3. Numerical Methodology

3.1 Finite Volume Method

The numerical method is based on a finite volume discretization on non-orthogonal boundary-fitted grids with a staggered arrangement of the variables. A grid with equidistant nodes is used everywhere, except near the melt/crystal/meniscus tri-junction and near the solid surfaces, where the grids are refined. The SIMPLE algorithm is used for the coupling of pressure and velocity fields. The governing equations are approximated for each control volume using a second-order accurate central difference scheme for the diffusive terms, and the QUICK scheme for the convective term. For the time integration a fully implicit method of second-order accuracy is applied. The simulations are proceeded up to 600 s. In each time step, the iteration process is continued until the residual values of all variables have reached convergence, *i.e.*, dropped six orders of magnitude. To ensure a maximum Courant number of about unity in each control volume and time step, a time step of Δt=0.02 s is used.

3.2 Grid Testing Calculations

An important issue for the quality of the numerical simulations with low-Reynolds number k-ε turbulence model is the choice of the grid. Three grid levels were used for the testing calculation: a coarse grid consisting of 580,237 control volumes with 2-3 nodes in the boundary layer, a moderate grid consisting of 68, 2871 control volumes with 3-4 nodes in the boundary layer, and a fine grid consisting of 1,465,422 control volumes with 4-5 nodes in the boundary layer. Calculations were performed taking the following case: ΔT=10K, Ω_s=15rpm, Ω_c=0rpm.

Figure2 presents the isothermal surfaces at T= 1517.2 K(a-c) and isovel surfaces at V=0.016m/s(d-f) at t = 400 s for three sets of grids. Owing to the interacting forces associated with different length scales in the LEC melt, the fluid flow is non-

axisymmetric [17]. It is seen that all the three sets of grids can predict the non-axisymmetric temperature and velocity fields in the melt.

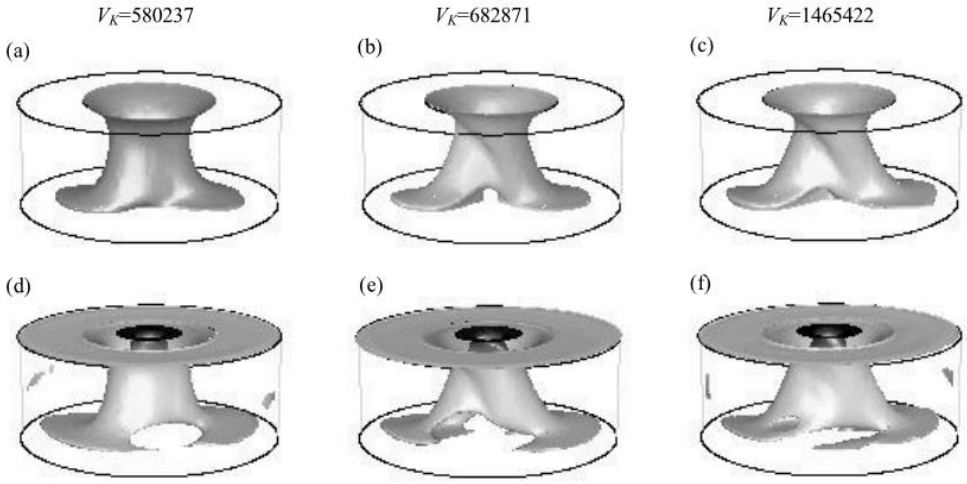

Figure 2. Isothermal Surfaces at T= 1517.2 K (a-c) and Isovel Surfaces at V=0.016m/s (d-f) at t = 400 s for Three Sets of Grids. ΔT=10K, Ωs=15rpm, Ωc=0rpm

Figure3 shows histories of the temperatures and corresponding power spectra at point N_3 for three sets of grids. Because of the competition between buoyancy, Marangoni force, centrifugal force and the Coriolis force, the flux of the warm melts passing through a certain point varies with time, leading to the temperature fluctuation at this point. All the three sets of grids can predict the temperature fluctuation characteristics. However, both the amplitudes and the frequencies of the temperature fluctuation at any point are grid dependent. The standard deviation and the main frequency of temperature fluctuation at point N_3 for three sets of grids are listed in Table 1. It is found from the table that the results obtained with the coarse grid (580,237 control volumes) is quite different from the ones obtained with the moderate grid(68, 2871 control volumes) and fine grid(1,465,422 control volumes), for which the results are in qualitative agreement. So the grid of 68, 2871 control volumes is good enough to obtain a grid independent solution and is chosen for the present study.

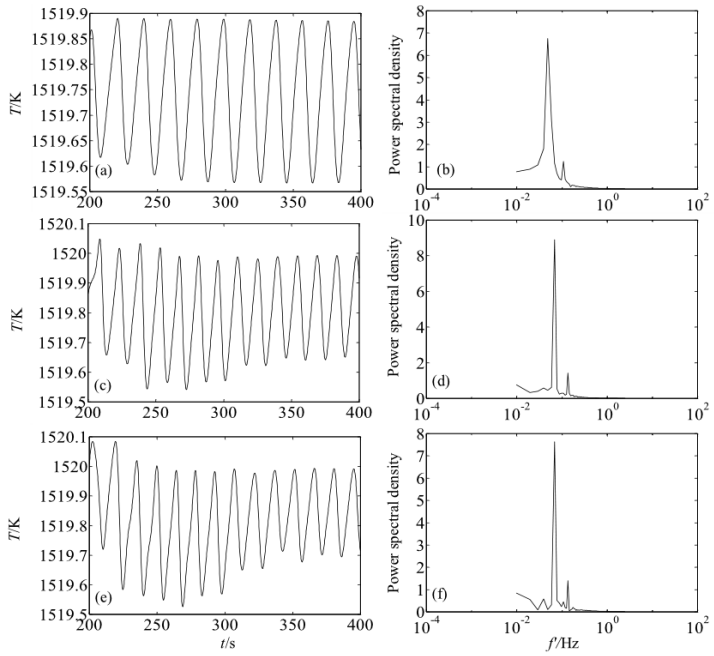

Figure 3. Histories of the Temperatures and Corresponding Power Spectra at Point N3 for VK=580237(a)(b), VK=682871(c)(d), VK=1465422 (e)(f). Calculations were Performed Taking the Following Values: ΔT=10K, Ωs=15rpm, Ωc=0rpm

Table 1. Standard Deviation and the Main Frequency of Temperature at Point N3, ΔT=10K, Ωs=15rpm, Ωc=0rpm

Grid number	580237	682871	1465422
Standard deviation (S/K)	0.12	0.15	0.15
Main frequency of the temperature (f'/Hz)	0.055	0.07	0.07

4. Results and Discussion

4.1 Modeling of the Mass, Heat and Momentum Transport Characteristics

In order to verify the mathematical model and numerical methodology for the simulation of mass, heat and momentum transport characteristics in the LEC melt of GaAs, the calculation of the turbulent flow and heat transfer in the CZ melt in Lee's experiments [5] with similar physical model is performed. Mercury melt that has a similar Pr (Pr≈0.025) number with GaAs melt was used as the working fluid. Lee *et al*. carried out experiments under different parametric conditions, varying parameters such as rotation rate of the crucible and the temperature difference. From all experiments, four cases were selected for the numerical simulations, called Case A to Case D:

Case A: H/Rc=0.4,Ωc=0.628 rad/s,ΔT=1.47 K;

Case B: H/Rc=0.4,Ωc=0.628 rad/s,ΔT=11.59 K;

Case C: H/Rc=1,ΔT=2.5K,Ωc=0.314rad/s;

Case D: H/Rc=1,ΔT=2.5K,Ωc=1.256rad/s.

The maximum T_{max}, the minimum T_{min}, and the standard deviation S of temperature fluctuations at monitor point T_{a1} ((r, z, θ) = (10 mm, 2.5 mm, π)) from the present simulations and measurements in Ref. (Lee *et al*., 1999) are listed in Table 2. One can see that the numerical results are in good agreement with the

experimental results except for T_{max} at T = 11.59 K. The larger value of T_{max} obtained from experiment may be an occasional value due to the disturbance [5]. The peak-to-peak temperature oscillation amplitudes ΔT_{max} at monitor points $T_{b2}(r, z,\theta)$=(63mm, 10 mm,π/3) and$T_{d2}(r, z,\theta)$= (63mm, 42 mm,π/3) from simulations in this work and measurements presented in Ref. [5] are listed in Table 3. It can be found that the ΔT_{max} from numerical results are in good agreement with that obtained in the experiments for lower and higher crucible rotation rates.

Table 2. Maximum, Minimum, and Standard Deviation of Temperature at Monitor Point Ta1 from Simulations in this Work and Measurements Presented in Ref. [5]. H/Rc=0.4,Ωc=0.628 rad/s

	ΔT=1.47K		ΔT=11.59K	
	Simulation	Experiment	Simulation	Experiment
T_{max}/K	20.16	20.17	39.5	40.7
T_{min}/K	20.03	20.05	36.8	37
S /K	0.025	0.025	0.7	0.7

Table 3. The Peak-to-Peak Temperature Oscillation Amplitude ΔTmax, t (K) at Monitor Points Tb2 and Td2 from Simulations in this Work and Measurements Presented in Ref. [5]. H/Rc=1,ΔT=2.5K

	Ω_c=0.314 rad/s		Ω_c=1.256 rad/s	
	Simulation	Experiment	Simulation	Experiment
T_{b2} point	1.2	1.2	1.5	1.5
T_{d2} point	1.1	1.2	0.7	0.75

So the mathematical model and numerical methodology adopted in the present simulation are effective for the prediction of mass, heat and momentum transport characteristics in the LEC melt of GaAs.

4.2 Modeling of the Dopant Transport in the In-Doped LEC Gaas Melt

In order to verify the mathematical model and numerical methodology for the simulation of dopant transport in the In-doped LEC GaAs melt, the calculation of the turbulent flow, heat and dopant transport in the In-doped LEC GaAs melt in He and Kou's experiments[2] with the conventional LEC process is performed. Figure 4 shows the axial InAs concentration profile in the crystal grown with the targeted composition of C_s=0.04mol% InAs obtained from the present simulations and measurements in Ref. (He *et al.*, 2000). Due to the segregation, the InAs concentration increase in the axial direction, and the present simulation quantitatively predicted the increase as measured by him and Kou. Figure 5 shows the dopant segregation in the crystal grown with the targeted composition of C_s=0.1mol% InAs. Again, the simulation results are in good agreement with the experimental results.

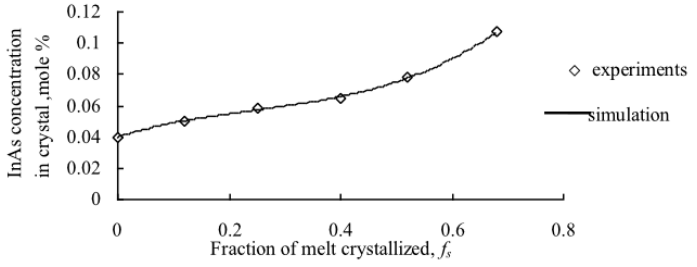

Figure 4. Axial Inas Concentration Profile in the Crystal Grown with the Targeted Composition of Cs=0.04mol% Inas Obtained from the Present Simulations and Measurements

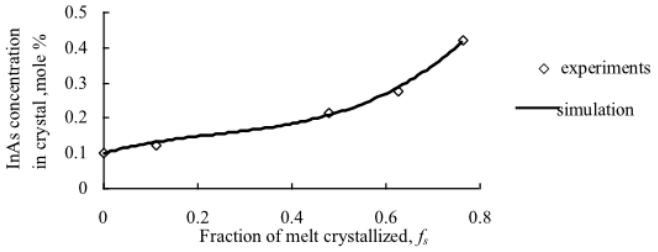

Figure 5. Axial Inas Concentration Profile in the Crystal Grown with the Targeted Composition of Cs=0.1mol% Inas Obtained from the Present Simulations and Measurements

5. Conclusion

A three-dimensional and time-dependent turbulent mathematical model is established for the mass, heat, momentum and dopant transport in the LEC melt of In-doped GaAs. The moderate grid (68, 2871 control volumes) is good enough to obtain a grid independent solution and is chosen. A low-Reynolds number k-ε turbulent model is proved to be suitable for capturing accurately the essentials of flow and heat transfer driven by temperature gradient and rotation in the melt. The mathematical model and numerical methodology are also validated for the simulation of dopant transport in the In-doped LEC GaAs melt. Owing to the interacting forces associated with different length scales in the LEC melt, the fluid flow is non-axisymmetric. Because of the competition between buoyancy, Marangoni force, centrifugal force and the Coriolis force, the flux of the warm melts passing through a certain point varies with time, leading to the temperature fluctuation in the melt. Due to the segregation, the InAs concentration increase in the axial direction.

Acknowledgement

This study is supported by the National Natural Science Foundation of China (No. 51306201) and the Jiangsu Province Key Laboratory of Aerospace Power Systems (No. APS-2013-04).

References

[1] R. Faiez and M. Asadian, "Modeling of convective interactions and crystallization front shape in GaAs/LEC growth process", Journal Cryst. Growth, vol. 311, **(2009)**, pp. 688-694.
[2] J. He and S. Kou, "LEC growth of In-doped GaAs with bottom solid feeding", Journal Cryst. Growth, vol. 216, **(2000)**, pp. 21-25.
[3] J. He and S. Kou, "Liquid-encapsulated Czochralski growth of Ga1-xInxAs single crystals with uniform compositions", Journal Cryst. Growth, vol. 308, **(2007)**, pp. 10-18.
[4] W. P. Jones and B. E. Launder, "The prediction of laminarization with a two-equation model of turbulence", International Journal Heat Mass Transfer, vol. 15, **(1972)**, pp. 301-314.
[5] Y. S. Lee and Ch. H. Chun, "Transition from regular to irregular thermal wave by coupling of natural convection with rotating flow in Czochralski crystal growth", Journal Cryst. Growth, vol. 197, **(1999)**, pp. 297-306.
[6] M .W. Li, W. Hu, N. Chen, D. Zeng and Z. Tang, "Numerical analysis of LEC growth of GaAs with an axial magnetic field International", Journal of Heat and Mass Transfer, vol. 45, **(2002)**, pp. 2843–2851.

[7] N. Miyazaki and Y. Kuroda, "Finite element analysis of dislocation density during bulk single crystal growth", Journal Cryst. Growth, vol. 196, **(1999)**, pp. 62-66.
[8] P. O. Nam and K. W. Yi, "Simulation of the thermal fluctuation according to the melt height in a CZ growth system", Journal Cryst. Growth, vol. 312, **(2010)**, pp. 1453-1457.
[9] N. Nikitin and V. Polezhaev, "Direct simulations and stability analysis of the gravity driven convection in a Czochralski model", Journal Cryst. Growth, vol. 230, **(2001)**, pp. 30-39.
[10] P. Rudolph and M. Jurisch, "Bulk growth of GaAs: an overview", Journal Cryst. Growth, vol. 198-199, **(1999)**, pp. 325-335.
[11] O. V. Smirnova and V. V. Kalaev, "3D unsteady numerical analysis of conjugate heat transport and turbulent/laminar flows in LEC growth of GaAs crystals", International Journal Heat Mass Transfer, vol. 47, **(2004)**, pp. 363-371.
[12] O. V. Smirnova, V. V. Kalaev, Y. N. Makarov, C. C. F. Rotsch, M. Neubert and P. Rudolph, "3D computations of melt convection and crystallization front geometry during VCz GaAs growth", Journal Cryst. Growth, vol. 266, **(2004)**, pp. 67-73.
[13] P. Spalart and S. Allmaras, "A one-equation turbulence model for aerodynamic flows", Technical Report AIAA-92-0439, American Institute of Aeronautics and Astronautics, **(1992)**.
[14] W. Q. Tao, "Numerical Heat Transfer, the second ed", Xi'an Jiao Tong University Press, Xi'an, **(2001)**.
[15] D. Vizman, S. Eichler, J. Friedrich and G. Müller, „Three-dimensional modeling of melt flow and interface shape in the industrial liquid-encapsulated Czochralski growth of GaAs", Journal Cryst. Growth, vol. 266, **(2004)**, pp. 396-403.
[16] E. V. Yakovlev, O. V. Smirnova, E. N. Bystrova, V. V. Kalaev, C. F. Rotsch, M. Neubert, P. Rudolph and Y. N. Makarov, "Modeling analysis of VCz growth of GaAs bulk crystals using 3D unsteady melt flow simulations", Journal of Crystal Growth, vol. 250, **(2003)**, pp. 195-202.
[17] E. V. Yakovlev, V. V. Kalaev, I. Y. Evstratov, C. F. Rotsch, M. Neubert, P. Rudolph and Y. N. Makarov, "Global heat and mass transfer in vapor pressure controlled Czochralski growth of GaAs crystals", Journal Cryst. Growth, vol. 252, **(2003)**, pp. 26-36.
[18] Y. F. Zou, G. X. Wang, H. Zhang, V. Prasad and D. F. Bliss, "Macro-segregation, dynamics of interface and stresses in high pressure LEC grown crystals", J. Cryst. Growth, vol. 180, **(1997)**, pp. 524-533.

